THE JOURNAL OF BIOLOGICAL CHEMISTRY VOL. 285, NO. 49, pp. 38204–38213, December 3, 2010
© 2010 by The American Society for Biochemistry and Molecular Biology, Inc. Printed in the U.S.A.

Structures of the Human GTPase MMAA and Vitamin B_{12}-dependent Methylmalonyl-CoA Mutase and Insight into Their Complex Formation*[S]

Received for publication, August 23, 2010 Published, JBC Papers in Press, September 28, 2010, DOI 10.1074/jbc.M110.177717

D. Sean Froese[‡§], Grazyna Kochan[‡], João R. C. Muniz[‡], Xuchu Wu[§], Carina Gileadi[‡], Emelie Ugochukwu[‡], Ewelina Krysztofinska[‡], Roy A. Gravel[§], Udo Oppermann[‡¶1], and Wyatt W. Yue[‡2]

From the [‡]Structural Genomics Consortium, University of Oxford OX3 7DU, United Kingdom, the [§]Department of Biochemistry & Molecular Biology, University of Calgary T2N 4N1, Canada, and the [¶]Botnar Research Centre, NIHR, Oxford Biomedical Research Unit, Oxford OX3 7LD, United Kingdom

Vitamin B_{12} (cobalamin, Cbl) is essential to the function of two human enzymes, methionine synthase (MS) and methylmalonyl-CoA mutase (MUT). The conversion of dietary Cbl to its cofactor forms, methyl-Cbl (MeCbl) for MS and adenosyl-Cbl (AdoCbl) for MUT, located in the cytosol and mitochondria, respectively, requires a complex pathway of intracellular processing and trafficking. One of the processing proteins, MMAA (methylmalonic aciduria type A), is implicated in the mitochondrial assembly of AdoCbl into MUT and is defective in children from the *cblA* complementation group of cobalamin disorders. To characterize the functional interplay between MMAA and MUT, we have crystallized human MMAA in the GDP-bound form and human MUT in the apo, holo, and substrate-bound ternary forms. Structures of both proteins reveal highly conserved domain architecture and catalytic machinery for ligand binding, yet they show substantially different dimeric assembly and interaction, compared with their bacterial counterparts. We show that MMAA exhibits GTPase activity that is modulated by MUT and that the two proteins interact *in vitro* and *in vivo*. Formation of a stable MMAA-MUT complex is nucleotide-selective for MMAA (GMPPNP over GDP) and apoenzyme-dependent for MUT. The physiological importance of this interaction is highlighted by a recently identified homoallelic patient mutation of MMAA, G188R, which, we show, retains basal GTPase activity but has abrogated interaction. Together, our data point to a gatekeeping role for MMAA by favoring complex formation with MUT apoenzyme for AdoCbl assembly and releasing the AdoCbl-loaded holoenzyme from the complex, in a GTP-dependent manner.

In humans, vitamin B_{12} (cobalamin, Cbl) is the cofactor for two enzymes: cytosolic methionine synthase and mitochondrial methylmalonyl-CoA mutase (MUT,[3] also known as MCM), utilizing methylcobalamin (MeCbl) and adenosylcobalamin (AdoCbl) as cofactor forms, respectively. Because of the different subcellular locations of the two enzymes and distinct modifications required to produce usable forms of Cbl, an exquisite subcellular pathway has evolved for the uptake, processing and delivery of Cbl to its destination enzymes. The essential nature of intracellular Cbl processing is underscored by the presence of inherited defects in intermediate metabolic steps, giving rise to the rare metabolic disorders of methylmalonic aciduria and homocystinuria (1). These defects, designated complementation groups *cblA-G* and *mut*, represent mutations in genes encoding the Cbl processing and utilization enzymes (2–4). Among them, three complementation groups, *cblA*, *cblB*, and *mut*, correspond to defects of the mitochondrial enzymes MMAA, MMAB, and MUT, respectively (5–7). MMAB is an ATP:cob(I)alamin adenosyltransferase (ATR) that transfers 5′-deoxyadenosyl from ATP to Cbl forming AdoCbl and delivers it to MUT (5, 8). MMAA, whose function is not clearly defined, has been shown to be integral to MUT function and AdoCbl synthesis (9).

MUT catalyzes the AdoCbl-dependent rearrangement of methylmalonyl-CoA (mmCoA) to succinyl-CoA (sCoA). The structure of MUT from *Propionibacterium shermanii* (*ps*MUT) has been determined (10–12). It contains an N-terminal TIM barrel accommodating the substrate binding site, a C-terminal AdoCbl binding domain, and an interdomain linker (10). Whereas this work has enhanced enormously our understanding of bacterial MUT structure and function, its application to human MUT (hMUT; 60% sequence identity) is hindered by

* The Structural Genomics Consortium is a registered charity (Number 1097737) funded by the Canadian Institutes for Health Research, the Canadian Foundation for Innovation, Genome Canada through the Ontario Genomics Institute, GlaxoSmithKline, Karolinska Institutet, the Knut and Alice Wallenberg Foundation, the Ontario Innovation Trust, the Ontario Ministry for Research and Innovation, Merck and Co., Inc., the Novartis Research Foundation, the Swedish Agency for Innovation Systems, the Swedish Foundation for Strategic Research, and the Wellcome Trust. D. S. F. acknowledges funding support by the CIHR Training Program in Genetics, Child Development and Health at the University of Calgary. R. A. G. acknowledges funding support by the Canadian Institutes for Health Research Grant MGP-44353.

The atomic coordinates and structure factors (codes 2WWW, 3BIC, 2XIJ, and 2XIQ) have been deposited in the Protein Data Bank, Research Collaboratory for Structural Bioinformatics, Rutgers University, New Brunswick, NJ (http://www.rcsb.org/).

[S] The on-line version of this article (available at http://www.jbc.org) contains supplemental Figs. S1–S4.

[1] To whom correspondence may be addressed. Fax: 44-0-1865-617571; E-mail: udo.oppermann@sgc.ox.ac.uk.

[2] To whom correspondence may be addressed. Fax: 44-0-1865-617571; E-mail: wyatt.yue@sgc.ox.ac.uk.

[3] The abbreviations used are: MUT, methylmalonyl-CoA mutase; MMAA/B, methylmalonic aciduria type A/B; aa, amino acid; AdoCbl, adenosylcobalamin; ATR, adenosyltransferase; mCoA, malonyl-CoA; MeCbl, methylcobalamin; mmCoA, methylmalonyl-CoA; MW, molecular weight; PFA, paraformaldehyde; sCoA, succinyl-CoA.

the different structural configuration of the human enzyme. Unlike *ps*MUT, which is a heterodimer of one catalytic (α) and one acatalytic subunit (β) (13), hMUT is a homodimer with two catalytic (α) subunits per dimer (14).

Likewise, MeaB, the *Methylobacterium extorquens* ortholog of human MMAA (hMMAA), has also been crystallized (15). MeaB is a homodimer, with the C-terminal ~70 amino acids (aa) critical for dimerization. Each subunit contains a central G-domain encompassing the GTPase active site, typical of the G3E family of P-loop GTPases to which it belongs (16). The N-terminal ~50 aa extension, whose function is not readily apparent, was predicted to interact with MUT (15). Indeed, *in vitro* interaction has been demonstrated between *M. extorquens* MeaB and MUT by native-PAGE and isothermal titration calorimetry (17, 18), and between the *Escherichia coli* orthologs YgfD and Sbm by size exclusion chromatography (19). Additionally, the energetics of the binding interaction were dependent on the liganded state of MUT (apo *versus* holo) and MeaB (apo or GDP/GTP-bound) (17, 18). A role for MeaB has been recently proposed in gating AdoCbl transfer to MUT in order to discriminate against the binding of inactive Cbl forms, in a manner dependent upon GTP binding and hydrolysis (20). These results suggest that the human proteins hMMAA and hMUT might functionally interact in a similar manner.

In this study we determine, by x-ray crystallography, the structures of hMMAA and hMUT. We show that both proteins are homodimeric in native state albeit with different modes of dimeric assembly compared with their bacterial counterparts. We show further that hMMAA and hMUT interact *in vitro* and *in vivo* and that this interaction is nucleotide-selective for hMMAA and apoenzyme-dependent for hMUT and is associated with stimulation of hMMAA GTPase activity by hMUT. Finally, we show that complex formation and GTPase stimulation are abrogated in hMMAA with the G188R patient mutation.

EXPERIMENTAL PROCEDURES

Materials—Nucleotides, Antibodies, AdoCbl, and Malonyl-CoA (mCoA) were purchased from Sigma-Aldrich. C-terminally Flag-tagged MMAA in pCMV-Entry vector (pMMAA-Flag, TC101283) was purchased from OriGene. Affinity purified anti-hMUT antibody was prepared by immunizing mice against a protein fragment (aa 1–371) containing a C-terminal His_6 tag expressed from pET28a (Novagen). The antibody was blot affinity purified using immobilized hMUT as antigen (21).

Cloning, Expression, and Purification of Recombinant Proteins—A DNA fragment encoding N-terminally truncated (aa 73–424) hMMAA (IMAGE clone 40017263) was subcloned into the vector pNIC28-Bsa4 (GenBank^{TM} accession EF198106). A DNA fragment encoding N-terminally truncated (aa 12–750) hMUT (IMAGE clone 3908548) was subcloned into the vector pNIC-CTHF (GenBank^{TM} accession EF199844). Both plasmids were expressed in BL21(DE3)R3-Rosetta *E. coli* cells grown in TB medium with 50 μg/ml kanamycin, with induction by 0.5 mM IPTG overnight at 37 °C (hMMAA), or induction by 1 mM IPTG overnight at 18 °C (hMUT). Cell pellets were harvested, homogenized in lysis buffer (50 mM HEPES pH 7.5, 10 mM imidazole, 500 mM NaCl, 5% glycerol) with the Emulsiflex C3 homogenizer, and insoluble material removed by centrifugation. The supernatant was purified by affinity (Ni-NTA; Qiagen) and size-exclusion (Superdex 200; GE Healthcare) chromatography. Purified hMMAA protein was treated with His-tagged TEV protease (1:20 mass ratio) overnight at 4 °C and passed over 1 ml Ni-NTA resin. Purified hMUT protein was desalted into low salt buffer (50 mM HEPES pH 7.5, 50 mM NaCl, 5% glycerol) and further purified by ion exchange chromatography (Resource Q; GE Healthcare). Proteins were concentrated (~20 mg/ml) and stored in either Buffer A (10 mM HEPES pH 7.5, 500 mM NaCl, 5% glycerol; hMMAA) or Buffer B (10 mM HEPES pH 7.5, 100 mM NaCl, 5% glycerol; hMUT) at −80 °C. The $hMMAA_{G188R}$ mutant was made using the QuikChange site-directed mutagenesis kit (Strategene) following manufacturer's instructions, and confirmed by DNA sequencing. Mutant protein was purified as with wild-type hMMAA.

Crystallization and Structure Determination—Crystals were grown by vapor diffusion at 20 °C in sitting drops containing 50 nl of protein and 100 nl mother liquor for hMMAA, or 100 nl protein and 50 nl mother liquor for hMUT. The mother liquor conditions for hMMAA and hMUT crystals are summarized in Table 1. To crystallize hMMAA, protein (10 mg/ml) was pre-incubated with 1.5 mM GMPPNP. To crystallize hMUT-AdoCbl binary complex, protein (19.6 mg/ml) was preincubated with 250 μM AdoCbl. To yield a ternary complex, protein (19.6 mg/ml) was preincubated with 250 μM AdoCbl and 2.5 mM mCoA. Crystals were cryo-protected in mother liquor containing 25% (v/v) ethylene glycol and flash-cooled in liquid nitrogen. Diffraction data were collected at the Diamond Light Source beamlines I02 and I03, and processed using the CCP4 program suite (22) (Table 1).

Initial phases were calculated by molecular replacement with *PHASER* (23) using as search models the structure of *M. extorquens* MeaB for hMMAA (PDB code 2QM7) (15) or the structure of *ps*MUT for hMUT (PDB code 4REQ) (12). ARP/wARP (24) was used for automated model building, followed by iterative cycles of REFMAC5 (25) refinement and model building with COOT (26). Calculation of difference Fourier maps revealed unambiguous electron density for AdoCbl and mCoA in the corresponding hMUT complexes (supplemental Fig. S1). For hMMAA, an attempt to co-crystallize GMPPNP resulted in GDP bound in the crystal (supplemental Fig. S1), likely due to the absence of Mg^{2+} in the crystallization condition, which is required to coordinate with the γ-phosphate (27). As observed previously (28), GDP may have originated as a contaminant from commercial sources of GMPPNP, reported as only 80% pure. Statistics for data collection and refinement are summarized in Table 1.

Kinetics of hMMAA GTP Hydrolysis—The GTPase activity of hMMAA (20 μM) was determined in the presence of various concentrations of GTP (50–5000 μM) by the Enzchek Phosphate Assay (Invitrogen), following manufacturer's instructions and using a POLARstar Omega plate reader (BMG Labtech). Initial velocities for each substrate concentration were calculated and GraphPad Prism 5.0 (GraphPad Software Inc.) was used to calculate the K_m and V_{max} by nonlinear regres-

TABLE 1
Data collection and refinement of crystallographic data

	hMMAA	$hMUT_{apo}$	$hMUT_{holo}$	$hMUT_{ter}$
Crystallization condition	32.5% LMW PEG smear[a], 0.2 M NH_4NO_3, 0.1 M Na-cacodylate pH 5.0	1.6 M Na/K-phosphate, 0.1 M HEPES pH 7.5	30% PEG3350, 0.1 M Bis-Tris pH 5.5, 0.3 M $(NH_4)_2SO_4$	20% PEG3350, 0.1 M Bis-Tris pH 5.5, 0.1 M $(NH_4)_2SO_4$
PDB ID	2WWW	3BIC	2XIJ	2XIQ
Resolution (Å)	27.43-2.64	37.42-2.60	47.80-1.95	53.91-1.95
Space group	$P4_2$	$P2_1$	$C222_1$	$P2_12_12_1$
Unit cell				
a,b,c (Å)	149.43,149.43,69.06	103.75,95.15,119.16	59.36,137.72,198.40	75.75,143.72,163.24
β (°)	90.00	108.31	90.00	90.00
Molecules/a.u.[b]	4	2	1	2
R_{merge}	7.0 (61.0)[c]	12.2 (69.8)	7.5 (51.7)	10.7 (68.0)
Completeness (%)	99.8 (100.0)	99.6 (97.3)	98.1 (97.6)	99.3 (97.3)
$I/\sigma(I)$	10.2 (2.0)	9.5 (1.6)	13.3 (2.5)	9.8 (2.0)
Multiplicity	4.0 (3.8)	3.6 (2.8)	3.8 (3.9)	4.4 (4.1)
Reflections	45149	67606	55496	128995
R_{cryst}/R_{free} (%)	18.4/22.2	21.8/24.3	15.8/19.9	16.1/20.1
Rmsd				
Bond (Å)/angle (°)	0.013/1.350	0.008/1.121	0.016/1.593	0.015/1.577
B factors (Å²)				
Protein/solvent/ligand	85.14/98.46/68.37	41.50/30.96/56.71	17.36/31.11/20.84 (48.51)[d]	15.97/51.87/35.18 (81.4)[d]
Atoms				
Protein/solvent/ligand	8921/87/155	10664/84/4	5464/528/173	11043/1106/362

[a] A mixture of PEG 300, 400, 550MME, 600, 1000.
[b] a.u., asymmetric unit.
[c] Data from the highest-resolution shell are shown in parentheses.
[d] In $hMUT_{holo}$ and $hMUT_{ter}$ structures, the ligand B-factors shown are for the cobalamin group and the 5′-deoxyadenosyl group (in brackets).

sion analysis. k_{cat} was calculated with the formula $k_{cat} = V_{max}/[E_{total}]$. The effect of hMUT (apo or holoenzyme) was determined by preincubating the complex (20 μM each protein) for 5 min on ice before initiating the GTPase assay.

Size Exclusion Chromatography—Analytical gel filtration was performed on a Superdex 200 HiLoad 10/30 column (GE Healthcare) pre-equilibrated with Buffer C (50 mM HEPES pH 7.5, 300 mM KCl, 2.5 mM $MgCl_2$, 5% glycerol). The column was calibrated using carbonic anhydrase (29 kDa), bovine serum albumin (66 kDa), alcohol dehydrogenase (150 kDa), and apoferritin (443 kDa) (Sigma) as MW standards.

Immunoprecipitation and Immunoblotting—HepG2 cells were transfected with pCMV-hMMAA-Flag, pCMV-Flag or pCMV-$hMMAA_{G188R}$-Flag using a nucleofection system (Amaxa), according to the manufacturer's instructions. After 48 h of incubation, cells were treated with 1% paraformaldehyde (PFA) at 37 °C for 20 min to cross-link protein complexes *in situ*, following which the cells were resuspended in lysis buffer (1% Nonidet P-40, 0.5% deoxycholine, 150 mM NaCl, 50 mM Tris-HCl, pH 7.5) for 1 h and then centrifuged at 10,000 × *g* for 10 min. The supernatant was incubated with anti-Flag antibody for 20 min then incubated with protein-G-agarose (Qiagen) overnight. To recover the pellet, the mixture was centrifuged at 1500 × *g* for 2 min. The antibody-bound protein was resuspended, heated at 95 °C for 20 min to release the protein from cross-linking, and immunoblotted with anti-Flag or anti-hMUT antibodies.

RESULTS

Homodimeric Assembly of hMUT and Comparison to psMUT—The structure of hMUT has been determined in the apoenzyme at 2.60 Å resolution ($hMUT_{apo}$), in binary complex with AdoCbl at 1.95 Å resolution ($hMUT_{holo}$), and in ternary complex with AdoCbl and the substrate analog malonyl-CoA (mCoA; lacking a branching methyl group) at 1.95 Å resolution (*h*MUT_{ter}) (Table 1). hMUT crystallized as a homodimer (Fig. 1*a*), consistent with its solution state (supplemental Fig. S2). Each hMUT monomer features a two-domain structure as observed for the α-subunit of *ps*MUT (60% sequence identity), namely a large substrate-binding TIM barrel (N-domain; Fig. 1*a*, *blue*) connected to a small AdoCbl-binding domain (C-domain; Fig. 1*a*, *pink*) via a ~100 aa inter-domain linker (Belt; Fig. 1*a*, *yellow*), with the active site situated at the N/C-domain interface. Although hMUT and *ps*MUT monomers superimpose well (rmsd < 2.0 Å), the two proteins differ substantially in their mode of dimeric assembly. The hMUT homodimer adopts a square cuboidal shape (Fig. 1, *a* and *c*), where the two AdoCbl-binding domains are positioned on the same square face (Fig. 1*c*, *white arrows*) with the entrances of the two substrate channels at opposing sides, close to the central grooves at the dimer interface (Fig. 1*c*, *black arrows*). *ps*MUT, by contrast, forms an $\alpha\beta$ heterodimer where cofactor and substrate binding regions are found only in the catalytic α subunit but not the acatalytic β-subunit (Fig. 1, *b* and *d*). As a result, hMUT has two active sites per dimer, whereas *ps*MUT has only one (10). Furthermore, the *ps*MUT heterodimer is more compact (shorter dimensions at the square face) and has less extensive surface grooves at the subunit interface than the hMUT homodimer (compare Fig. 1, *c* and *d*). These observations suggest that hMUT may interact with its functional partner(s) in a different manner than *ps*MUT and other heterodimeric MUT orthologs *e.g. M. extorquens* MUT.

hMUT Adopts an Induced-fit Mechanism for Binding Cofactor and Substrate—Previously, comparison of the *ps*MUT structures in the holo and ternary states revealed a substrate-induced conformational rearrangement of the protein (11). However, in the absence of an apo structure, it could not be assessed whether cofactor-induced structural rearrangement occurs. Here, the structures of $hMUT_{apo}$, $hMUT_{holo}$,

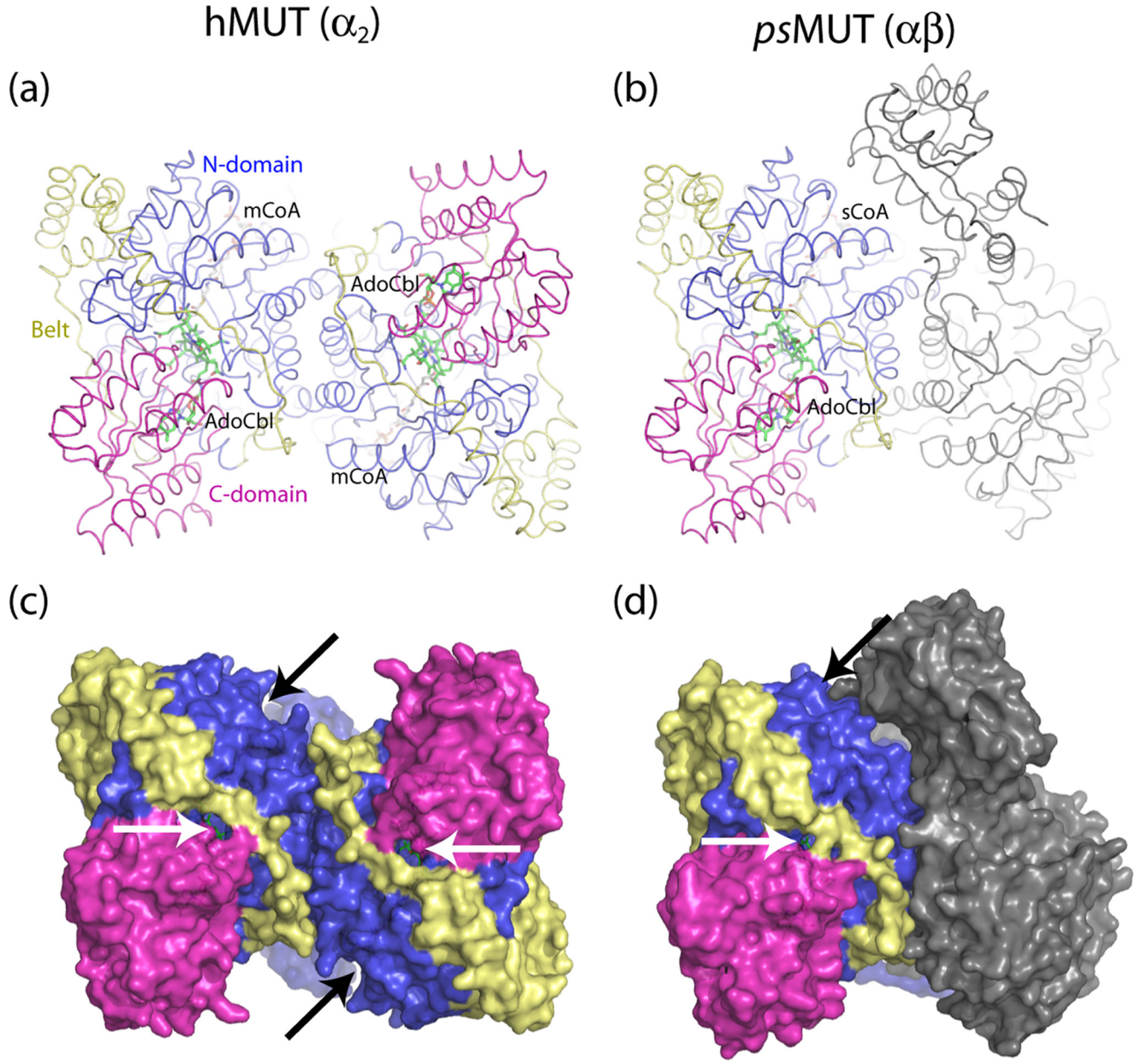

FIGURE 1. **Dimeric assembly of human and bacterial MUT.** Cartoon and surface representations of the hMUT homodimer (*a*, *c*) and *ps*MUT heterodimer (*b*, *d*, PDB code 4REQ). Catalytic subunits (α) are colored according to domain architecture (N-domain, *blue*; C-domain, *magenta*; interdomain belt, *yellow*). The bacterial regulatory subunit (β) is colored *gray*. In *panels c* and *d*, the cofactor binding pocket and substrate binding channel are indicated by *white arrow* and *black arrow*, respectively. *mCoA*, malonyl-CoA; *Cbl*, cobalamin; *sCoA*, succinyl-CoA.

and $hMUT_{ter}$ provide snapshots of both the substrate and AdoCbl binding events in the human enzyme. Structural rearrangements upon cofactor binding can be identified by comparison of the $hMUT_{apo}$ and $hMUT_{holo}$ structures, which reveal significant outward displacement (rmsd ~2.5 Å) in several C-domain helices (Fig. 2*a*), while the N-domain remains largely stationary (rmsd ~0.6 Å). This creates an induced-fit pocket at the domain interface for binding AdoCbl, by positioning the His-627 imidazole to coordinate with the Cbl cobalt atom, rearranging the Leu-674 and Ala-675 side chains that would otherwise sterically clash with one of the cofactor propionamide tails, and burying the Cbl dimethylbenzimidazole (DMB) tail in a glycine-rich hydrophobic cavity (Fig. 2*a*). These conformational changes enable the "base-off/His-on" cofactor configuration, where the DMB tail, usually coordinated to the Cbl cobalt, is displaced by His-627 from hMUT, an important criterion for catalysis (10). In addition, the cofactor-binding pocket is shielded from the solvent exterior due to a reordering of the linker belt in $hMUT_{holo}$ (aa 500–505) that was flexible in $hMUT_{apo}$ (Fig. 2*c*, *top* and *middle*), while the substrate binding channel remains exposed via a long crevice (Fig. 2*d*, *top* and *middle*).

Comparison of the $hMUT_{holo}$ and $hMUT_{ter}$ structures reveal major Cα differences in the N-domain TIM barrel (Fig. 2*b*) upon substrate binding, similar to those observed in *ps*MUT. In contrast to the open substrate channel in $hMUT_{apo}$ and $hMUT_{holo}$, the N-domain TIM barrel tightens and constricts the channel pore in the $hMUT_{ter}$ structure (*arrows* in Fig. 2*b*),

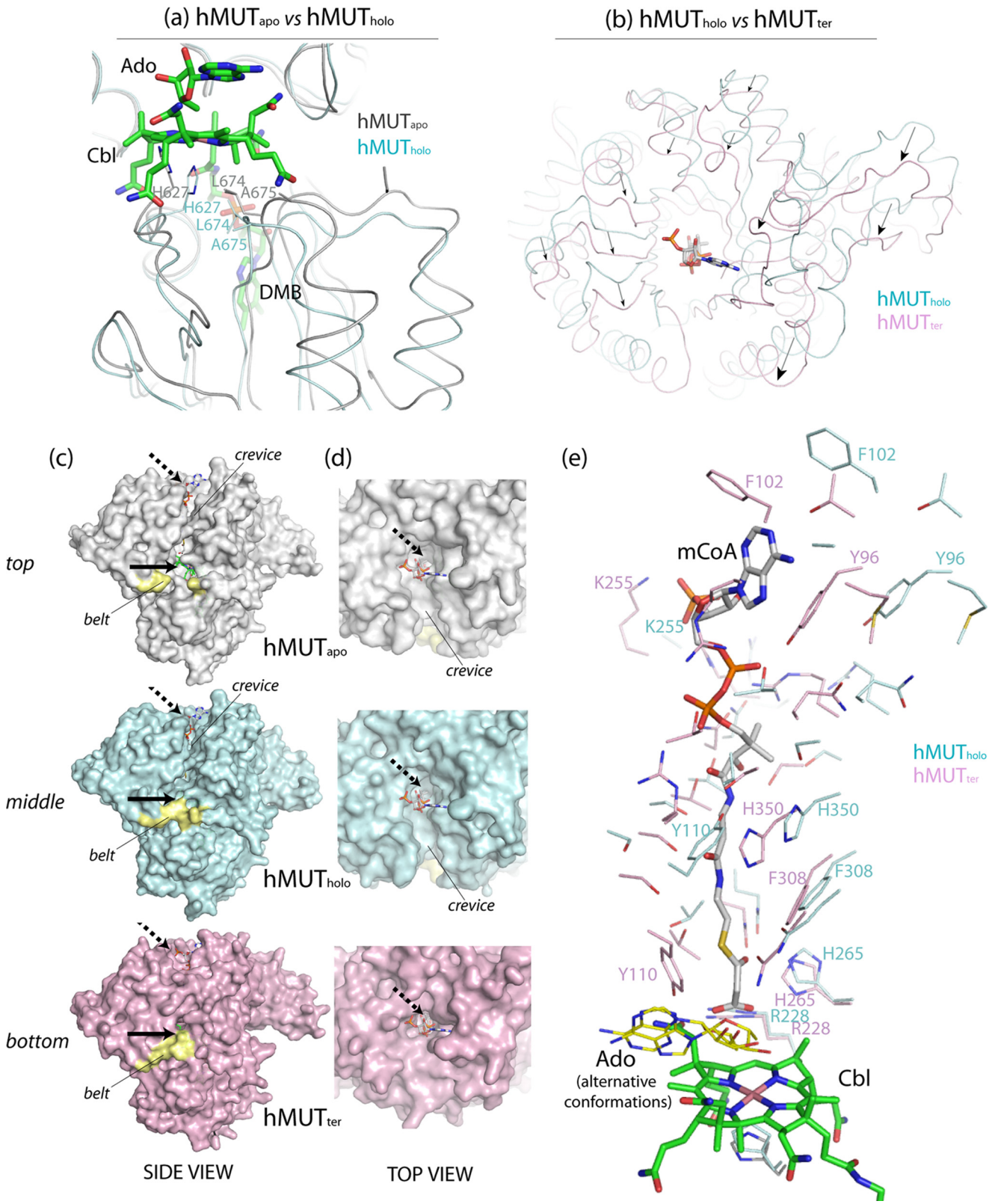

FIGURE 2. **Ligand-induced conformational changes in hMUT.** *a*, active site view of the $hMUT_{holo}$ structure (*cyan*), superimposed with the $hMUT_{apo}$ structure (*gray*). The bound AdoCbl molecule in the $hMUT_{holo}$ structure is shown in *green sticks*. *b*, Superposition of the $hMUT_{holo}$ (*cyan*) and $hMUT_{ter}$ (*pink*) structures, viewed from the entrance of the substrate binding channel (shown with substrate analog mCoA in *white sticks*). *Black arrows* indicate the displacement of secondary structures in the N-domain upon binding of mCoA. *c* and *d*, surface representation of the structures of $hMUT_{apo}$ (*top*), $hMUT_{holo}$ (*middle*), and $hMUT_{ter}$ (*bottom*), highlighting the substrate binding channel (*broken arrow*), cofactor binding pocket (*solid arrow*), and part of the flexible interdomain belt (*yellow*) that becomes ordered upon cofactor binding. For convenient comparison, molecules of mCoA and AdoCbl have been added to all panels. *e*, substrate binding channel of hMUT is shown with channel-lining residues in the $hMUT_{holo}$ (*cyan lines*) and $hMUT_{ter}$ (*pink lines*) structures. The bound substrate analog (mCoA) and cofactor (Cbl) are shown in *sticks*. Two alternative conformations of the cofactor 5′-deoxyadenosyl group (Ado), as revealed in the electron density map, are shown (*yellow*).

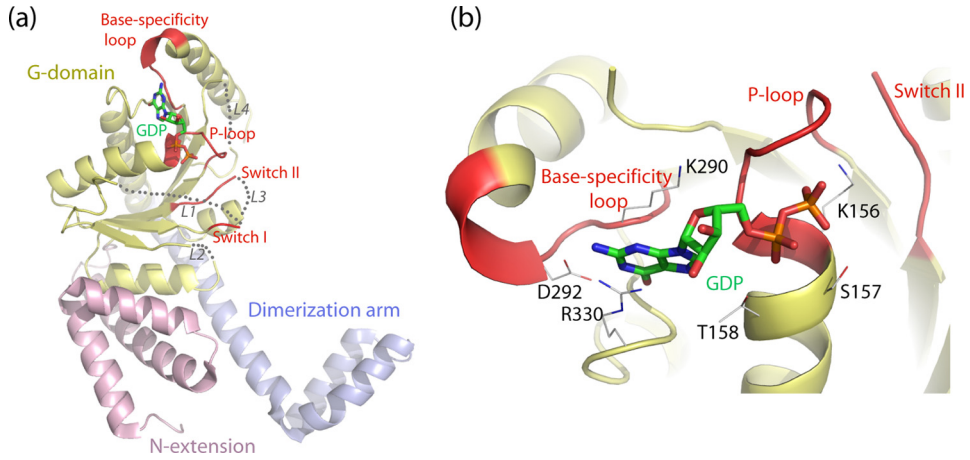

FIGURE 3. **Crystal structure of human MMAA.** *a*, structure of an hMMAA monomer consists of the N-extension (*pink*), the G-domain (*yellow*) harboring four conserved sequence motifs for P-loop GTPases (*red*), and the dimerization arm (*blue*). *b*, *cartoon representation* of the hMMAA nucleotide binding site, bound with GDP (in *sticks*). Residues forming polar interactions with GDP are shown in *lines*. Three conserved sequence motifs are colored *red*.

thereby sealing off the long crevice from the solvent exterior (Fig. 2, *c*, *bottom* and *d*, *bottom*). Consequently, this brings the highly-conserved residues lining the channel into close contact with the acyl-CoA substrate (Fig. 2*e*). Significantly, the phenolic side chain of the invariant Tyr-110 is shifted >8 Å from its position in the $hMUT_{apo}$/$hMUT_{holo}$ structures and, together with the invariant His-265 and Arg-228, positions the substrate carboxyl for catalysis. The $hMUT_{holo}$ and $hMUT_{ter}$ structures also differ in the orientation of the 5′-deoxyadenosyl moiety of the AdoCbl cofactor, which is covalently bonded (via the adenosyl methyl carbon) to the cobalt atom in the $hMUT_{holo}$ structure, but in the $hMUT_{ter}$ structure the C-Co bond is broken, thereby generating the cob(II)alamin radical, and displacing the 5′-deoxyadenosyl group to adopt at least two alternative, less-ordered conformations in proximity to the substrate (Fig. 2*e* and supplemental Fig. S3). Therefore, substrate binding induces structural rearrangement in the cofactor as well as the protein.

Structure of Nucleotide-bound hMMAA—The assembly of the AdoCbl cofactor into hMCM is predicted to involve a GTP-dependent interaction with hMMAA, a member of the G3E family of P-loop GTPases, based on the properties of their bacterial orthologs (20). To provide insight into the role of human MMAA, we have determined the structure of GDP-bound hMMAA at 2.5 Å resolution (Table 1). hMMAA crystallized as a homodimer, in line with solution studies (supplemental Fig. S2). Each hMMAA monomer (Fig. 3*a*) consists of a central 7-stranded G-domain (aa 143–330) harboring the four GTPase signature motifs (namely Switch I, Switch II, P-loop, and base specificity loop), flanked by an N-terminal extension (aa 75–142) and a C-terminal dimerization arm (aa 331–416). Several loops connecting the G-domain β-strands are disordered, suggesting their intrinsic flexibility. These include aa 182–197 (L1, Switch I motif), aa 212–220 (L2), aa 246–248 (L3, part of Switch II motif), and aa 268–279 (L4). The bound GDP was anchored in a surface groove via polar interactions with highly conserved sequence motifs in the base specificity loop (Lys-290, Asp-292) and P-loop (Lys-156, Ser-157, Thr-158) (Fig. 3*b*). In addition, hMMAA contributed a non-conserved arginine (Arg-330; Leu-243 in MeaB) to line a pocket for the guanine moiety which interacts with the hydroxyl group of the GDP-ribose. No Mg^{2+} ion was observed in the nucleotide pocket, suggesting that GDP binding is metal-independent.

hMMAA Dimer Has a More Open Configuration than MeaB—The topology of hMMAA is similar to that of the previously reported *M. extorquens* MeaB structure (15), as monomers of the two proteins can be superimposed with an rmsd of 2.78 Å (Fig. 4*a*). Like MeaB, hMMAA crystallizes as a homodimer, but the relative placement of the monomers differs between the two proteins. In MeaB, helix α12 from the C-terminal dimerization arm forms a ~30° bend at residue Ala-282, midway along the helix, while helix α12 in $hMMAA_{GDP}$ is much less distorted (<5° bend in the opposite direction at the equivalent residue Asn-363). As a result, the two helices following, α13 and α14, are displaced by >10 Å away from the protein core in hMMAA compared with the equivalent helices in MeaB. In both structures, the dimerization arm (α12- α14) is closely intertwined with its equivalent arm from the neighboring subunit, and therefore the relative displacement of helices α13 and α14 impacts directly on the overall shape and dimensions of the resultant dimer. Significantly, superimposing the hMMAA and MeaB dimers using one monomeric subunit reveals dramatically different positional arrangements for the second subunit (supplemental Fig. S4). Consequently, $hMMAA_{GDP}$ dimerizes via the dimerization arms only (Fig. 4*b*, *top*) while the central G-domains from both subunits are oriented away from each other (Fig. 4*b*, *bottom*), hence adopting an open U-shaped configuration. By contrast, MeaB dimerizes using the dimerization arms and G-domains from both subunits (Fig. 4*c*), which results in a more closed configuration with a central cavity.

hMMAA Is a P-loop GTPase Modulated by hMUT—The presence of GTPase signature motifs in the central, G-domain of hMMAA suggests that it binds and hydrolyzes GTP. To assess its putative GTPase activity, we incubated recombinant hMMAA with increasing concentrations of GTP and monitored the time-dependent increase in P_i produced. Michaelis-Menten kinetics revealed an unexpectedly high K_m of 1210 ± 330 μM, along with the more expected catalytic constant (k_{cat}) of 0.030 ± 0.003 min^{-1} (Table 2)(Fig. 5*a*), the latter consistent with the bacterial ortholog MeaB (k_{cat} = 0.039 min^{-1})(18). Interestingly, when assayed in the presence of $hMUT_{apo}$, the catalytic efficiency (k_{cat}/K_m) of hMMAA increased more than 80-fold, due to both tighter binding (K_m = 74 ± 8 μM) and increased activity (k_{cat} = 0.15 ± 0.01 min^{-1}) (Table 2) (Fig. 5*a*), indicating a functional association between hMMAA and hMUT. Surprisingly, the addition of $hMUT_{holo}$ resulted in a

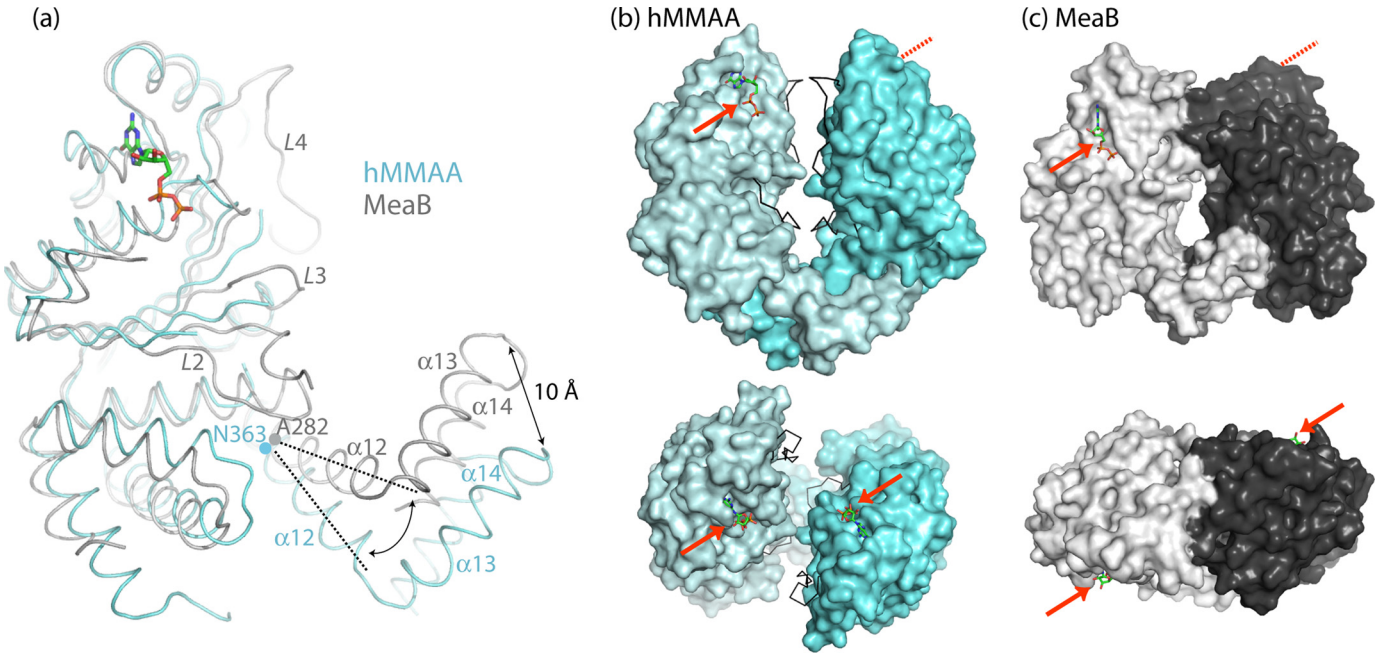

FIGURE 4. **Dimer assembly in hMMAA and MeaB.** *a*, Cα-superposition of hMMAA (*cyan*) and MeaB (*gray*) monomeric subunits, highlighting several loops in the G-domain (*L2–L4*) that are ordered in the MeaB structure, and the relative displacement of the dimerization arms of the two structures. *b* and *c*, surface representations of the hMMAA and MeaB homodimers, highlighting the positions of the nucleotide binding site of each subunit (*red arrows*). The bound GDP is shown in *sticks*. The two subunits of each dimer are colored in *light* and *dark shades* of *cyan* (hMMAA) or *gray* (MeaB). In *panel b*, the ordered loops *L2–L4* in MeaB structure are added onto the structure of hMMAA to illustrate the more complete polypeptide.

TABLE 2
Effect of hMUT on the GTPase activity of hMMAA

hMMAA	hMUT	K_m	V_{max}	k_{cat}	Catalytic efficiency	Stimulation
		μM	*nmol P_i/min*	min^{-1}	k_{cat}/K_m	
wt	None	1210 ± 330	0.019 ± 0.002	0.030 ± 0.003	2.48×10^{-5}	Reference
wt	Apo	74 ± 8	0.092 ± 0.002	0.15 ± 0.01	2.03×10^{-3}	82-fold[a]
wt	Holo	185 ± 28	0.023 ± 0.001	0.037 ± 0.001	2.00×10^{-4}	8-fold[a]
G188R	None	610 ± 156	0.019 ± 0.002	0.031 ± .0003	5.08×10^{-5}	Reference
G188R	Apo	993 ± 243	0.025 ± 0.002	0.040 ± 0.004	4.02×10^{-5}	None[b]

[a] Change in catalytic efficiency compared to reference (wt hMMAA, no hMUT).
[b] Change in catalytic efficiency compared to reference ($hMMAA_{G188R}$, no hMUT).

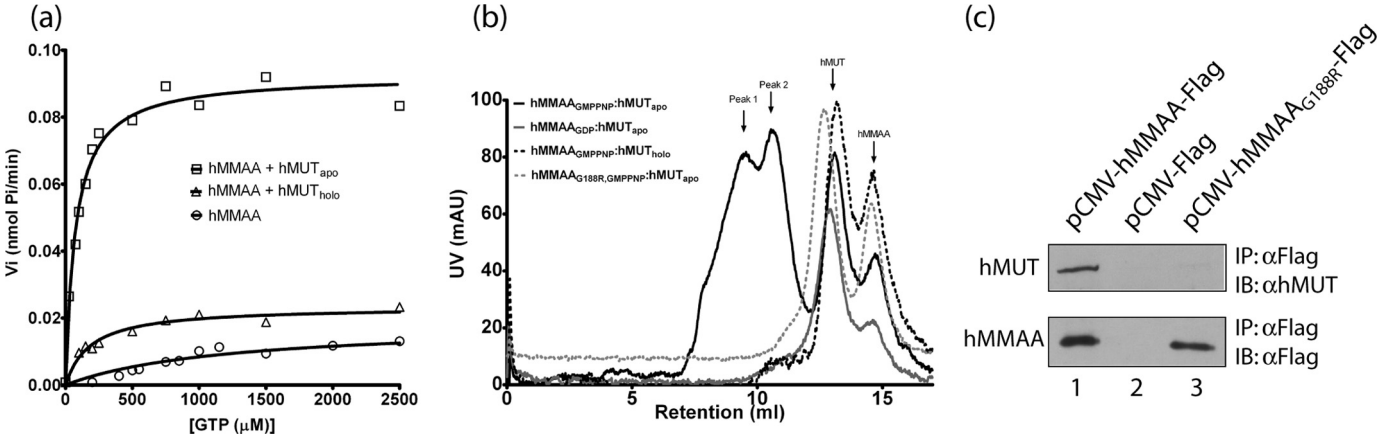

FIGURE 5. **Functional and physical interactions between hMMAA and hMUT.** *a*, effect of hMUT on the GTPase activity of hMMAA. Reactions were performed by incubating hMMAA with $hMUT_{apo}$ (*square*), $hMUT_{holo}$ (*triangle*), or without hMUT (*circle*). Kinetic parameters of GTP hydrolysis are shown in Table 2. *b*, gel filtration profile on a HiLoad 10/30 Superdex 200 column. The samples run are $hMMAA_{GMPPNP}$:$hMUT_{apo}$ mixture (*black line*), $hMMAA_{GDP}$:$hMUT_{apo}$ mixture (*gray line*), $hMMAA_{GMPPNP}$:$hMUT_{holo}$ (*black dashed line*), and $hMMAA_{G188R,GMPPNP}$:$hMUT_{apo}$ (*gray dashed line*). The two complex peaks as well as individual protein peaks are labeled. *c*, *in vivo* hMMAA-hMUT interaction. pCMV-hMMAA-Flag (*lane 1*), pCMV-Flag control (*lane 2*), or pCMV-$hMMAA_{G188R}$-Flag (*lane 3*) was transfected into HepG2 cells, cross-linked with 1% PFA, immunoprecipitated (*IP*) with anti-Flag antibody, and immunoblotted (*IB*) with anti-hMUT or anti-Flag antibody to identify hMUT and hMMAA, respectively.

less pronounced increase in the catalytic efficiency of hMMAA, by only 8-fold (Table 2)(Fig. 5*a*), suggesting that the cofactor state of hMUT directly influences its interaction with hMMAA. Additionally, we tested $hMMAA_{G188R}$, a recombinant hMMAA variant mimicking a homozygous mutation in a *cblA* patient (29). The GTPase activity of $hMMAA_{G188R}$ alone

was similar to wild-type levels; however, unlike wild-type hMMAA, it was not stimulated by the addition of $hMUT_{apo}$ (Table 2), suggesting the G188R mutation may interfere with the functional interaction between hMMAA and hMUT.

Physical Interaction of hMMAA-hMUT—To test whether hMUT and hMMAA interact directly, analytical size-exclusion chromatography was employed (Fig. 5*b*). Both hMUT and hMMAA migrated independently with apparent MW of 196 kDa and 78 kDa, respectively, consistent with homodimeric assembly in each case (supplemental Fig. S2). A mixture of $hMUT_{apo}$ and hMMAA preincubated with GMPPNP eluted with early, higher-MW species in addition to the individual protein dimer peaks (Fig. 5*b*, $hMMAA_{GMPPNP}$:$hMUT_{apo}$). The early species consist of two subpopulations, peaks 1 and 2, corresponding to 1410 kDa and 740 kDa, with a leading shoulder suggesting still higher MW species. SDS-PAGE analysis confirmed co-elution of hMUT and hMMAA from these peaks (data not shown), indicating complex formation. The presence of individual dimer peaks eluting after the high MW species suggests an equilibrium between the complexes and their protein components. Interestingly, the complexes require pre-bound GTP/GMPPNP for their formation, because in the absence of nucleotide (data not shown) or when a mixture of $hMUT_{apo}$ and hMMAA preincubated with GDP was analyzed, no early peaks were observed (Fig. 5*b*, $hMMAA_{GDP}$:$hMUT_{apo}$). Additionally, no complex was visualized when AdoCbl was pre-bound to hMUT and mixed with $hMMAA_{GMPPNP}$ (Fig. 5*b*, $hMMAA_{GMPPNP}$:$hMUT_{holo}$), suggesting that $hMUT_{holo}$ interacts less favorably with hMMAA than $hMUT_{apo}$, a finding consistent with our GTPase data. Finally, while $hMMAA_{G188R}$ migrated independently as a dimer similar to wild-type (supplemental Fig. S2), it did not form a complex with $hMUT_{apo}$ after pre-incubation with GMPPNP (Fig. 5*b*, $hMMAA_{G188R,GMPPNP}$:$hMUT_{apo}$).

Interaction between hMMAA and hMUT *in vivo* was confirmed by detection of hMUT following immunocapture of Flag-tagged hMMAA (hMMAA-Flag) from hMMAA-Flag-transfected HEPG2 cells (Fig. 5*c*). Cell lysates were treated with a cross-linking agent, immunoprecipitated with anti-Flag antibody, and then immunoblotted. A band corresponding to hMUT was detected in cells expressing hMMAA-Flag (*lane 1*), but not in Flag-only cells (*lane 2*) or cells expressing $hMMAA_{G188R}$-Flag (*lane 3*). Together, these data demonstrate that hMMAA and hMUT form a complex *in vivo* and *in vitro*, which is abolished with the G188R mutation in hMMAA.

DISCUSSION

Despite having only two Cbl-dependent enzymes, mammals have deployed a complex pathway for the cellular uptake and assembly of Cbl into its destination enzymes. However, the biochemical properties of some individual components in this complex pathway and the molecular basis underlying their enzymatic functions are not well understood. Previous work on bacterial orthologs, including MUT from *P. shermanii* and MUT and MeaB from *M. extorquens*, have become the paradigm for predicting the biochemical behavior and interaction of human MUT and MMAA. In this study, we have examined the structures of hMUT and hMMAA, demonstrating a nucleotide-dependent interaction of the two proteins and a gating behavior of hMMAA toward cobalamin binding of hMUT, and confirm the occurrence of a protein complex in cells *in vivo* but not in a GTPase-active mutant protein carrying the G188R substitution. We further demonstrate unique structural and biochemical differences between these two human proteins and their bacterial counterparts, which have mechanistic implications for their functional interaction and role in cofactor assembly.

Human MMAA-MUT Interaction Is Ligand-dependent and Ligand-selective—Consistent with the presence of GTPase signature motifs and enzyme activities of the *M. extorquens* MeaB (17, 18) and *E. coli* YgfD (19) orthologs, our GTP hydrolysis assay demonstrated moderate GTPase activity for hMMAA. This activity is enhanced by hMUT, as observed for MeaB (18), but unlike MeaB, it is enhanced in a cofactor-dependent manner with 80-fold stimulation by $hMUT_{apo}$ *versus* 8-fold by $hMUT_{holo}$. The modulation of hMMAA activity by hMUT confirms a functional association between these two proteins. Further, by size exclusion chromatography, a stable complex of recombinant hMMAA and hMUT could be detected in a nucleotide-selective (GMPPNP- but not GDP-bound) and apoenzyme-dependent manner. Pre-binding AdoCbl to hMUT also interfered with complex formation even with GMPPNP-bound hMMAA. This interaction was confirmed *in vivo* by the ability to co-immunoprecipitate the two proteins from fibroblast homogenates treated with a cross-linking agent. Complex formation has been reported for the orthologous *E. coli* pair (YgfD-Sbm) using size-exclusion chromatography and similar co-immunoprecipitation from cell extracts (19) and for the *M. extorquens* pair (MeaB-MUT) using native-PAGE (17, 18). However, the preference for the hMUT apoenzyme over holoenzyme in forming the stable human complex was not observed with the bacterial orthologs and is in keeping with the more pronounced enhancement of GTPase activity by hMMAA in the presence of $hMUT_{apo}$ compared with $hMUT_{holo}$. The nucleotide-selective nature of hMMAA in the interaction assay, also observed in the *E. coli* YgfD-Sbm complex (19), indicates a dependence on GTP binding or hydrolysis for complex formation, and may be used to target hMMAA to the hMUT apoenzyme in preference to the already functional AdoCbl-loaded holoenzyme. Our data are in keeping with the recently proposed GTP-dependent "gating" role for MeaB in screening for the active AdoCbl cofactor for incorporation into MUT (20). Therefore, the unique nucleotide-binding prerequisite to the formation of the $hMMAA_{GMPPNP}$-$hMUT_{apo}$ complex may be relevant physiologically to the acquisition of AdoCbl by the MUT apoenzyme to form the holoenzyme in the human system.

hMMAA and hMUT Dimeric Assembly Has Implications for Their Interaction—As an initial step toward structurally characterizing an hMMAA-hMUT complex, we have crystallized the individual proteins hMMAA and hMUT in various liganded forms. The two proteins show a strong evolutionary conservation between the bacterial and human proteins in all aspects of their structural folds, domain architecture and catalytic machinery (10, 15), consistent with their moderate sequence homology (~50%) and, for the MUT enzymes, the

preservation of an induced-fit mechanism to communicate the binding of cofactor and substrate with the active site catalytic machinery. Nevertheless, inspection of the hMMAA and hMUT homodimers, which had been expected to be their biological oligomeric state (30, 31), reveals significantly different modes of dimeric assembly compared with the corresponding bacterial proteins.

The different hMMAA/MeaB dimeric configurations are the result of relative displacements in their dimerization arms, a polypeptide region less conserved at the sequence level and distant from the G-domain, and hence unlikely to be nucleotide-dependent. Consequently, the more open hMMAA dimer positions its two nucleotide-binding sites more closely to each other (~20 Å) than does the MeaB dimer (50 Å). Also, the hMMAA dimer exposes a much larger surface at the dimer interface than the MeaB dimer with its more constricted central cavity. For MUT, the different dimeric configurations between the human and *P. shermanii* structures are primarily due to subunit compositions. The *ps*MUT $\alpha\beta$ heterodimer (13) harbors only one active site contributed from the catalytic α subunit. This contrasts with the hMUT α_2 homodimer, shown structurally as a square cuboid, harboring two active sites (one from each α subunit) positioned on the same cuboid face. The homodimeric arrangement is also predicted for *E. coli* (32) and mouse (33).

These structural configurations lead to predictions about the nature of the oligomeric complexes formed between hMMAA and hMUT. Our $hMMAA_{GMPPNP}$-$hMUT_{apo}$ complex from size exclusion chromatography may represent supramolecular species built from the core structure of 2 hMMAA dimers: 1 hMUT dimer (MW ~352 kDa). Hence the 740 kDa and 1410 kDa peaks might represent 2 units (calculated mass 704 kDa) and 4 units (1408 kDa) of the core structure, respectively. The 2:1 stoichiometry is compatible with our structural data, where the nucleotide binding sites and Switch (I and II) motifs from both subunits of the hMMAA dimer are juxtaposed close enough in the central cavity to be contacted simultaneously by one subunit of the hMUT dimer. This differs from the complex formed by *M. extorquens* MUT and MeaB, which saturated at a ratio of 1 MeaB dimer:1 MUT dimer (18). It is not unexpected that the bacterial orthologs may adopt a different stoichiometric relationship and binding mode, because *M. extorquens* MUT is a heterodimer and has a smaller accessible surface than hMUT (~45,000 *versus* 53,000 $Å^2$) and requires only 1 mol of AdoCbl. The nature of the supramolecular complex formation is currently under investigation by co-crystallization and electron microscopy studies.

In the mitochondrial pathway for Cbl assimilation, AdoCbl synthesized by the MMAB adenosyltransferase from cob(I-I)alamin and ATP is transferred to MUT in a manner that involves, but has left enigmatic, a role for MMAA (34, 35). In the *M. extorquens* MeaB system, AdoCbl is transferred directly to MUT without release into the milieu. When GTP-bound MeaB is complexed with MUT, the selectivity for AdoCbl becomes very high, predicting a gating role for MeaB. Our hMUT and hMMAA dimeric structures, combined with the high-MW complexes formed *in vitro* and demonstrated to occur *in vivo*, raise similar questions regarding the stoichiometry between the hMUT dimer and its two functional partners. Human MMAB forms a homotrimer (36) that binds 2 mol of Cbl and 2 mol of ATP (37), and hence one trimer has the capacity to deliver 2 mol of AdoCbl to one hMUT homodimer. It is not known whether the delivery and/or loading of 2 mol of AdoCbl per hMUT homodimer requires one or two hMMAA dimer(s), although the 2 hMMAA: 1 hMUT core structure predicted from size exclusion chromatography suggests that each hMUT subunit is handled independently.

A Patient Mutation in hMMAA Abolishes Its Interaction with hMUT—To establish a physiological relevance for our observed hMMAA-hMUT interaction, we searched for patient mutations in hMMAA that abolish complex formation. To date, eight *hMMAA* missense mutations have been reported (6, 29, 38, 39), all of which were characterized biochemically in MeaB (15) except the recently identified homozygous G188R mutation (29). Unlike other *hMMAA* mutations shown to affect protein stability (15), $hMMAA_{G188R}$ can be expressed recombinantly as a soluble homodimer, and exhibits near wild-type GTPase activity, suggesting the mutation has no deleterious effects on its structure and stability. However, the $hMMAA_{G188R}$ GTPase activity is neither enhanced by hMUT nor can the mutant protein complex with hMUT, demonstrating that the mutation affects directly the robustness of its interaction with hMUT. Gly-188 is part of the Switch I motif in the G-domain, located at the dimer interface, and is disordered in our hMMAA structure. Switch I and II are signaling motifs that transduce GTP binding/hydrolysis with downstream effector proteins (40), so that their conformations may depend on whether hMMAA is bound with GTP and/or hMUT. Therefore, our analysis of the G188R mutant, the first characterized to affect hMMAA-hMUT interaction, extends previous suggestions that the MeaB N-terminal extension binds MUT by demonstrating here that the G-domain and the dimer interface of hMMAA are also involved in the interaction, and underscores the importance of the Switch motifs in the functional interplay between hMMAA and hMUT.

Proposed Model for hMMAA-mediated Cofactor Assembly into hMUT—Our studies lead to a model for the role of hMMAA in maintaining the functional integrity of hMUT. As proposed by Banerjee and co-workers (1, 20), GTP-bound MeaB distinguishes the transfer of authentic AdoCbl from ATR (bacterial ortholog of human MMAB) to MUT apoenzyme (gate-keeping) and screens for and removes oxidized Cbl from MUT (editing) in a GTP-dependent manner. Our results point to an evolutionary retention of a gate-keeping role for hMMAA, but with some significant differences. We speculate that, in the human system, AdoCbl binding releases hMUT from the hMMAA-hMUT complex in a GTP-dependent manner. Our results also suggest an importance of supramolecular complexes in this process, though at this time, their significance remains unclear. However, the pathological outcome of the G188R patient mutation underscores the essential role of these protein complexes in generating or maintaining functional hMUT. The benefit of the higher order complexes might be to sequester hMUT apoenzyme in proximity of an MMAB/ATR factory that would convert incoming Cbl to AdoCbl for concerted transfer to the hMMAA-hMUT complex. This would

minimize loss of AdoCbl to the mitochondrial milieu and would allow hMMAA to perform the gate-keeping function predicted for MeaB. This model, with release of functional hMUT holoenzyme after cofactor assembly, would be less attuned to hMMAA-mediated surveillance on the functional state of cofactor bound to MUT, as proposed for the MeaB-MUT system. It will be interesting to see if this editing function identified for MeaB extends to the human enzyme.

Acknowledgments—We thank the protein crystallography group for synchrotron data collection.

REFERENCES

1. Banerjee, R., Gherasim, C., and Padovani, D. (2009) *Curr. Opin. Chem. Biol.* **13,** 484–491
2. Rutsch, F., Gailus, S., Miousse, I. R., Suormala, T., Sagné, C., Toliat, M. R., Nürnberg, G., Wittkampf, T., Buers, I., Sharifi, A., Stucki, M., Becker, C., Baumgartner, M., Robenek, H., Marquardt, T., Höhne, W., Gasnier, B., Rosenblatt, D. S., Fowler, B., and Nürnberg, P. (2009) *Nat. Genet.* **41,** 234–239
3. Lerner-Ellis, J. P., Tirone, J. C., Pawelek, P. D., Doré, C., Atkinson, J. L., Watkins, D., Morel, C. F., Fujiwara, T. M., Moras, E., Hosack, A. R., Dunbar, G. V., Antonicka, H., Forgetta, V., Dobson, C. M., Leclerc, D., Gravel, R. A., Shoubridge, E. A., Coulton, J. W., Lepage, P., Rommens, J. M., Morgan, K., and Rosenblatt, D. S. (2006) *Nat. Genet.* **38,** 93–100
4. Coelho, D., Suormala, T., Stucki, M., Lerner-Ellis, J. P., Rosenblatt, D. S., Newbold, R. F., Baumgartner, M. R., and Fowler, B. (2008) *N. Engl. J. Med.* **358,** 1454–1464
5. Dobson, C. M., Wai, T., Leclerc, D., Kadir, H., Narang, M., Lerner-Ellis, J. P., Hudson, T. J., Rosenblatt, D. S., and Gravel, R. A. (2002) *Hum. Mol. Genet.* **11,** 3361–3369
6. Dobson, C. M., Wai, T., Leclerc, D., Wilson, A., Wu, X., Doré, C., Hudson, T., Rosenblatt, D. S., and Gravel, R. A. (2002) *Proc. Natl. Acad. Sci. U.S.A.* **99,** 15554–15559
7. Ledley, F. D., Lumetta, M., Nguyen, P. N., Kolhouse, J. F., and Allen, R. H. (1988) *Proc. Natl. Acad. Sci. U.S.A.* **85,** 3518–3521
8. Leal, N. A., Park, S. D., Kima, P. E., and Bobik, T. A. (2003) *J. Biol. Chem.* **278,** 9227–9234
9. Mahoney, M. J., Hart, A. C., Steen, V. D., and Rosenberg, L. E. (1975) *Proc. Natl. Acad. Sci. U.S.A.* **72,** 2799–2803
10. Mancia, F., Keep, N. H., Nakagawa, A., Leadlay, P. F., McSweeney, S., Rasmussen, B., Bösecke, P., Diat, O., and Evans, P. R. (1996) *Structure.* **4,** 339–350
11. Mancia, F., and Evans, P. R. (1998) *Structure.* **6,** 711–720
12. Mancia, F., Smith, G. A., and Evans, P. R. (1999) *Biochemistry* **38,** 7999–8005
13. Marsh, E. N., Harding, S. E., and Leadlay, P. F. (1989) *Biochem. J.* **260,** 353–358
14. Jansen, R., Kalousek, F., Fenton, W. A., Rosenberg, L. E., and Ledley, F. D. (1989) *Genomics* **4,** 198–205
15. Hubbard, P. A., Padovani, D., Labunska, T., Mahlstedt, S. A., Banerjee, R., and Drennan, C. L. (2007) *J. Biol. Chem.* **282,** 31308–31316
16. Leipe, D. D., Wolf, Y. I., Koonin, E. V., and Aravind, L. (2002) *J. Mol. Biol.* **317,** 41–72
17. Korotkova, N., and Lidstrom, M. E. (2004) *J. Biol. Chem.* **279,** 13652–13658
18. Padovani, D., Labunska, T., and Banerjee, R. (2006) *J. Biol. Chem.* **281,** 17838–17844
19. Froese, D. S., Dobson, C. M., White, A. P., Wu, X., Padovani, D., Banerjee, R., Haller, T., Gerlt, J. A., Surette, M. G., and Gravel, R. A. (2009) *Microbiol. Res.* **164,** 1–8
20. Padovani, D., and Banerjee, R. (2009) *Proc. Natl. Acad. Sci. U.S.A.* **106,** 21567–21572
21. Tang, W. J. (1993) *Methods Cell Biol.* **37,** 95–104
22. CCP4. (1994) *Acta Crystallogr. D Biol. Crystallogr.* **50,** 760–763
23. McCoy, A. J., Grosse-Kunstleve, R. W., Storoni, L. C., and Read, R. J. (2005) *Acta Crystallogr. D Biol. Crystallogr.* **61,** 458–464
24. Perrakis, A., Harkiolaki, M., Wilson, K. S., and Lamzin, V. S. (2001) *Acta Crystallogr. D Biol. Crystallogr.* **57,** 1445–1450
25. Murshudov, G. N., Vagin, A. A., and Dodson, E. J. (1997) *Acta Crystallogr. D Biol. Crystallogr.* **53,** 240–255
26. Emsley, P., and Cowtan, K. (2004) *Acta Crystallogr. D Biol. Crystallogr.* **60,** 2126–2132
27. Ruzheinikov, S. N., Das, S. K., Sedelnikova, S. E., Baker, P. J., Artymiuk, P. J., García-Lara, J., Foster, S. J., and Rice, D. W. (2004) *J. Mol. Biol.* **339,** 265–278
28. Batra, J. K., Lin, C. M., and Hamel, E. (1987) *Biochemistry* **26,** 5925–5931
29. Merinero, B., Pérez, B., Pérez-Cerdá, C., Rincón, A., Desviat, L. R., Martínez, M. A., Sala, P. R., García, M. J., miz-Echevarría, L., Campos, J., Cornejo, V., Del, Toro, M., Mahfoud, A., Martínez-Pardo, M., Parini, R., Pedrón, C., Peña-Quintana, L., Pérez, M., Pourfarzam, M., and Ugarte, M. (2008) *J. Inherit. Metab. Dis.* **31,** 55–66
30. Fenton, W. A., Hack, A. M., Willard, H. F., Gertler, A., and Rosenberg, L. E. (1982) *Arch. Biochem. Biophys.* **214,** 815–823
31. Kolhouse, J. F., Utley, C., and Allen, R. H. (1980) *J. Biol. Chem.* **255,** 2708–2712
32. Haller, T., Buckel, T., Rétey, J., and Gerlt, J. A. (2000) *Biochemistry* **39,** 4622–4629
33. Wilkemeyer, M. F., Crane, A. M., and Ledley, F. D. (1990) *Biochem. J.* **271,** 449–455
34. Fenton, W. A., and Rosenberg, L. E. (1981) *Biochem. Biophys. Res. Commun.* **98,** 283–289
35. Yamanishi, M., Vlasie, M., and Banerjee, R. (2005) *Trends Biochem. Sci.* **30,** 304–308
36. Schubert, H. L., and Hill, C. P. (2006) *Biochemistry* **45,** 15188–15196
37. Padovani, D., Labunska, T., Palfey, B. A., Ballou, D. P., and Banerjee, R. (2008) *Nat. Chem. Biol.* **4,** 194–196
38. Yang, X., Sakamoto, O., Matsubara, Y., Kure, S., Suzuki, Y., Aoki, Y., Sakura, N., Takayanagi, M., Iinuma, K., and Ohura, T. (2004) *Mol. Genet Metab.* **82,** 329–333
39. Lerner-Ellis, J. P., Dobson, C. M., Wai, T., Watkins, D., Tirone, J. C., Leclerc, D., Doré, C., Lepage, P., Gravel, R. A., and Rosenblatt, D. S. (2004) *Hum. Mutat.* **24,** 509–516
40. Vetter, I. R., and Wittinghofer, A. (2001) *Science* **294,** 1299–1304